*Article*

# Spatial and temporal variation of $NO_2$ vertical column densities (VCDs) over Poland: Comparison of the Sentinel-5P TROPOMI observations and the GEM-AQ model simulations

**Marcin Kawka [1]\* , Joanna Strużewska [1,2] and Jacek W. Kamiński [1,3]**

[1]   Institute of Environment Protection - National Research Institute, Poland;marcin.kawka@ios.edu.pl
[2]   Faculty of Building Services, Warsaw University of Technology, Poland; joanna.struzewska@is.pw.edu.pl
[3]   Institute of Geophysics, Polish Academy of Sciences, 01-452 Warsaw, Poland; jkaminski@ecoforecast.net
\*    Correspondence: marcin.kawka@ios.edu.pl;

**Abstract:** The TROPOMI instrument aboard Sentinel-5P is a relatively new, high-resolution source of information about atmosphere composition. One of the primary atmospheric trace gases that we can observe is nitrogen dioxide. Thanks to TROPOMI capabilities (high resolution and short revisit time), one can describe regional and seasonal $NO_2$ concentration patterns. So far, such patterns were analysed by either ground measurements (which were limited to specific locations and only to near-surface troposphere layer) and numerical models. This paper compares the TROPOMI and GEM-AQ derived vertical column densities (VCD) over Poland, focusing on large point sources. Although well established in atmospheric science, the GEM-AQ simulations are always based on emission data, which in the case of the energy sector were reported by stack operators. Also, we checked how cloudy conditions influence TROPOMI results. Finally, we tried to link the $NO_2$ column number densities with surface concentration using boundary layer height as an additional explanatory variable. Our results showed a general underestimation of $NO_2$ tropospheric column number density by the GEM-AQ model (compared to the TROPOMI). However, for the locations of the most significant point sources, we noticed a systematic overestimation by the GEM-AQ model (excluding spring and summer months when TROPOMI presents larger $NO_2$ VCDs than GEM-AQ). For the winter months, we have found TROPOMI $NO_2$ VCD results highly dependent on the choice of qa_value threshold.

**Keywords:** air pollution; $NO_2$; Sentinel-5P; TROPOMI; GEM-AQ; Poland

---

## 1. Introduction

Nitrogen oxides ($NO_x = NO + NO_2$) play a significant role in tropospheric chemistry processes. As oxidisers precursors, they contribute to the tropospheric ozone formation process. Most of $NO_x$ emissions are released as a form of NO molecules, but they quickly convert to $NO_2$. Thus, tropospheric $NO_2$ is commonly used as a more chemically stable proxy for $NO_x$ emissions [1]. There are two major types of $NO_x$ emissions - from road traffic and from industrial emissions, both of which originate from high-temperature combustion. The former is located at the earth surface and distributed proportionally to the road network, the latter at stacks located at bigger industrial incineration plants. For the most significant industrial $NO_x$ sources in Poland, stack height is roughly within the range of 100-300 meters. This paper focuses on large point emitters since they are an issue of great concern, and their environmental impact exceeds the local scale.

There are several methods for obtaining gridded $NO_2$ estimates on a larger than local scale. To name the most significant: chemical transport models (CTMs) or online chemical weather models, spatial interpolation of station-based measurements, empirical models (like Landuse regression LUR or socioeconomic regression [2]), remote sensing (satellite or much less common on an operational scale - aerial). Since each method has its intrinsic strengths and weaknesses, synergistic use of multiple sources of information and data-driven methods (also known as data assimilation or data fusion methods) is also gaining increasing attention [3,4].

Within the satellite remote sensing of atmospheric pollutants, significant progress has been made in recent decades. Starting from the first operational ultraviolet spectrometer, which was capable of delivering gridded data with a pixel size of 40 x320 $km^2$ (Global Ozone Monitoring Instrument - GOME) in 1995[5], followed by SCIAMACHY aboard Envisat (in 2002 [6]) and GOME-2 [7].

An undeniable advantage of progress in satellite remote sensing of tropospheric $NO_2$ concentration is the growing archive record of past measurements on a global scale. This makes them a powerful tool for spatial and temporal trend analysis[8–10] for environmental policy evaluation, industry and development assessment.

Applications of satellite-derived $NO_2$ column data archive covered numerous aspects like an assessment of the effectiveness of abatement strategies in China[11],[12],[13], tracking effects of economic cycles [14],[15],[16] , short-term regulations for events like the 2008 Beijing Olympic Games [17]. Thanks to high spatial resolution, satellite sensors play a vital role as an alternative (to bottom-up estimations) mean for estimating industrial emissions from large power plants, e.g. India [18], Greece [19] and South Africa [20] as well as from big cities in Mexico [21],France [22],USA [23]. Due to high spatial resolution, TROPOMI revealed information on emitters that were previously considered as challenging to estimate, e.g. compressor stations in Siberia [24], shipping emissions in African harbours [25], ONG exploration in Canada [26].

Many studies attempt to validate satellite-born TROPOMI $NO_2$ measurements using airborne [27], [28] and ground-based [29],[30],[31] spectrometers. The general conclusion is that it tends to underestimate $NO_2$ column number in highly polluted regions and overestimates in regions with low $NO_2$ tropospheric column content.

This paper aims to assess to what extent satellite-borne TROPOMI $NO_2$ measurement can be used to evaluate the results of the operational chemical weather forecast model (GEM-AQ). We also check if TROPOMI results are valid under cloudy weather winter conditions within a temperate climate. Finally, we attempt to link a satellite-borne tropospheric column with the near-surface concentrations using boundary layer depth as an additional regression variable.

## 2. Data and Methods

In this study, we have used TROPOMI observations, the GEM-AQ model 24-h forecast from the operational run and the observations from the national air quality monitoring network.

### 2.1. TROPOMI

TROPOMI, onboard Sentinel-5P satellite, is one of the most recently available instruments capable of monitoring $NO_2$ concentration in the atmospheric column. TROPOMI has a heritage to both the Ozone Monitoring Instrument (OMI) and the SCanning Imaging Absorption spectroMeter for Atmospheric CartograpHY (SCIAMACHY). The Sentinel-5P is intended to extend the data records of these missions as well as be a preparatory mission for the Sentinel-5. Thus, resolution and revisit time should be at least at the same level as for OMI and SCIAMACHY. Sentinel-5P performs, on average, one full and two partial scans over our area of interest per day.

The concentration retrieval algorithm (DOMINO, developed by KNMI) is based on the NO2 spectral properties in ultra-violet. It has previously been used for OMI [32], and with minor improvements, it has been adopted to TROPOMI data [33]. The retrieval algorithm uses several auxiliary atmospheric parameters within the processing, including the atmospheric mass factor (AMF).

To provide the necessary meteorological data, the profile shape from the TM5-MP model is used (run at 1 x 1°resolution [34] ). The surface albedo information is from a monthly OMI climatology (on a 0.5 x 0.5°resolution). Finally, a vertical column density (VCD) is provided by the algorithm in units $mol/m^2$ with a spatial resolution of approximately 7 x 3.5 $km^2$ (approx. 5.5 x 3.5 $km^2$ after 6 Aug 2019 [35]), aggregated as a tropospheric, stratospheric and total vertical column.

We used a level 2 product of TROPOMI (S5P_OFFL_L2__NO2), processed automatically by Copernicus Scientific data hub up to 5 days after sensing. Data were downloaded from the data hub using DHuSget 0.3.4 - an automatic sentinel data retrieving script. Within the level 2 product of TROPOMI, a quality assurance flag qa_value is provided for each pixel. This normalised flag is to be used as a threshold for discarding poor-quality retrievals from useful ones. Most authors use the default threshold value of 0.75 [2,3,36,37]. However, this highly limits the number of retrievals in temperate climate due to intensive cloud cover, especially during the winter months. According to TROPOMI ATBD [38], the value of 0.75 is recommended and should remove clouds and scenes covered by snow, ice and other problematic retrievals. However, the value of 0.5 is also proposed as still good enough for model-comparison studies. A lower threshold (thus a larger number of accepted retrievals) may be necessary if we still want to calculate monthly averages for the winter season. Discussion on the optimal value of qa_value will be given as examples in the results section. Therefore we decided to perform further processing using not only 0.75 but also 0.5 and 0.7 thresholds as a potential compromise.

Pixels that fulfil the above qa_value threshold requirement are also used to create masking layers, which are later used to calculate model-based monthly-average $NO_2$ column and model-based surface $NO_2$ concentration.

As the first processing step, TROPOMI data were regrided to GEM-AQ rectangular grid of size 300x470 and grid step 0.025°, using ESA Atmospheric Toolbox [39]. Secondly, regrided data were aggregated into monthly average raster. The term *monthly average*, although commonly used, may be a bit misleading in this context. Depending on location and time of the year - the monthly average may be an aggregate of 10 (in winter) to 40 (in the summer) cloud-free scans per pixel. TROPOMI NO2 column concentration is a scalar value. However, it is produced with averaging kernel - an averaging vector, which describes how sensitive the instrument was to $NO_2$ at a given time, altitude and location. The same averaging kernel was applied for the tropospheric $NO_2$ column calculated from the model data to make the GEM-AQ results comparable.
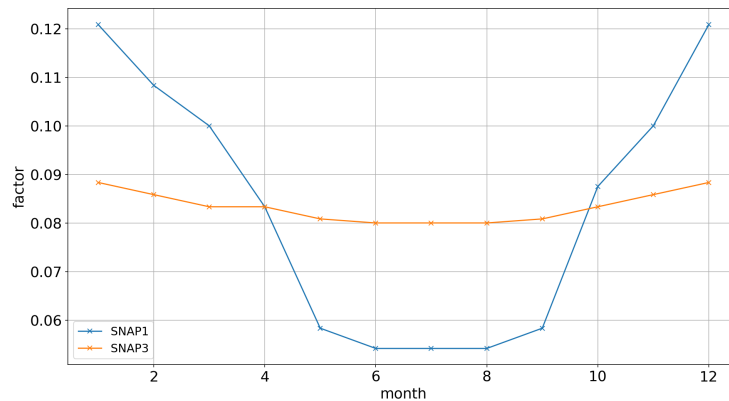
### 2.2. The GEM-AQ model

The GEM-AQ is a semi-Lagrangian chemical weather model in which air quality processes (chemistry and aerosols), tropospheric chemistry are implemented online in the operational weather prediction model, the Global Environmental Multiscale (GEM) [40] model, which was developed at Environment Canada. The Gas-phase chemistry mechanism used in the GEM-AQ model is based on a modified version of the Acid Deposition and Oxidants Model (ADOM)[41], where additional reaction in the free troposphere was included [42].

The GEM-AQ model instance, run at the Institute of Environment Protection (Poland), is an ensemble member in CAMS50 and hence undergoes evaluation against satellite observation in the scope of CAMS84. However, the model output requested for column calculations reaches only 5km. For the sake of this paper, the entire troposphere was used.

An earlier study based on the comparison of the tropospheric NO2 column with satellite observations GEM-AQ with SCIAMACHY observations addressed the spatial correlation with total $NO_x$ emission fluxes [43]. Since the TROPOMI instrument provides significantly better resolution than Envisat SCIAMACHY, it is now feasible to focus on particular categories of emissions. We chose to focus on significant industrial $NO_x$ sources because of the intensive contrast to the local $NO_2$ background.

Significant emission sources within the model are driven by emission data from the national emission inventory. These data are based on annual reporting obligation, which the facilities owners fulfil. Annual emissions are transformed into monthly emission rates using the weighting factor from annual emission profiles. Emission profiles are assigned to so-called SNAP categories [44]. In the case of $NO_x$ emissions over Poland, the largest point emissions are assigned to SNAPs 1 (energy production from coal-burning), 3 (non-energy manufacturing industry, e.g. concrete or steel production) and 7 (road transport). Traffic emissions are considered to be uniform during the whole year, while SNAPs 1 and 3 are expected to follow a typical pattern high in winter, low in summer (fig. 1)



**Figure 1.** Annual emission profiles for the energy production sector (SNAP 1) and non-energy manufacturing industry (SNAP 3)

The GEM-AQ model is set up to perform calculations using 28 vertical layers, out of which the lower 21 layers are classified as the troposphere. Troposphere averaging kernel is provided as an auxiliary variable of the TROPOMI level 2 $NO_2$ product. Averaging kernel values are provided at 35 levels of the TM5 model, which is the atmosphere model used within TROPOMI level 1 to level 2 processing [38]. TM5 averaging kernel is then linearly interpolated to GEM-AQ 28 levels (fig. 2). The $NO_2$ column number density is obtained for each layer using the following equation:

$$c_{NO_2,k} = f_k tnd_k \Delta z_k \tag{1}$$

where:
$f_k[ppb]$ - molecular mixing ratio
$tnd_k[molec/m^3]$ - total number density
$\Delta z_k[m]$ - layer depth

The $NO_2$ column number density in the whole tropospheric column is then calculated using column number density from each GEM-AQ layer and averaging kernel derived from TROPOMI image:

$$C_{NO_2} = \frac{1}{\sum_k avk_k} \sum_{k=1}^{28} c_{NO_2,k} avk_k \tag{2}$$

*2.3. Boundary layer depth*

The boundary layer is the lowest part of the troposphere, directly influenced by Earth surface and responds to these forcings in a short time scale [45]. Significant $NO_x$ emissions occur within the boundary layer, while a satellite sensor observes the whole tropospheric column integrated. Therefore, we expect boundary layer depth to be an additional variable that explains to what extent is the tropospheric column affected by concentrations from the boundary layer.
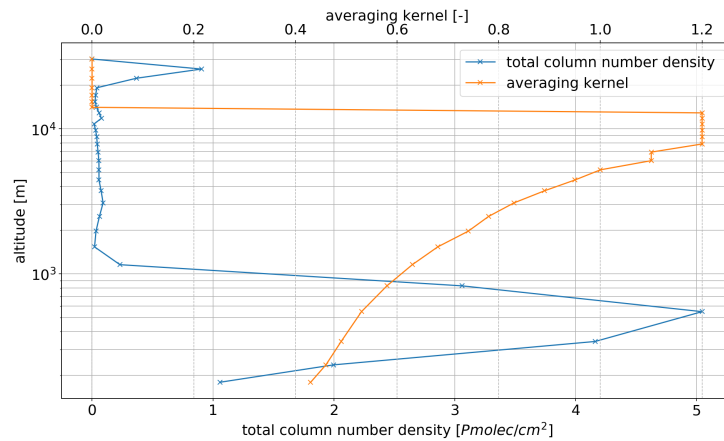
**Figure 2.** Example $NO_2$ vertical profile from GEM-AQ model and the TROPOMI-derived, troposphere averaging kernel, extracted at power plant stack location on 1st of April 2019

There are several ways of estimating boundary layer depth. Since GEM-AQ is an online chemical weather model with the meteorological component, we decided to use Gradient Richardson Number $R_i$ with a critical value of $R_c = 0.025$. We assume that when $R_i < R_c$ we are within the boundary layer and turbulent mixing is the dominant form of transport [45]. The Gradient Richardson Number is calculated as:

$$R_i = \frac{\frac{g}{\theta_v}\frac{\partial \theta_v}{\partial z}}{\left(\frac{\partial u}{\partial z}\right)^2 + \left(\frac{\partial v}{\partial z}\right)^2} \tag{3}$$

where $\theta_v$ is a virtual potential temperature, $u$ and $v$ are horizontal components of the velocity vector, resulting from the meteorological part of the GEM-AQ model.

### 2.4. Surface observations

Observations of surface $NO_2$ concentrations during 2019 were obtained from the Chief Inspectorate of Environment Protection, responsible for air quality monitoring in Poland. The dataset includes results from 112 automatic stations measuring with hourly time step.

## 3. Results

### 3.1. Overall Performance

Before detailed analysis, we performed a general linear regression analysis of TROPOMI $NO_2$ tropospheric column retrieval. We expect tropospheric columns retrieved using TROPOMI and the GEM-AQ model to be linearly correlated over the whole area of interest. Since we do not expect any additional bias, we assume that the noise is of Gaussian nature and the following regression equation is expected to be fulfilled:

$$N_{v,GEM}^{trop} = a * N_{v,TROPOMI}^{trop} + b \tag{4}$$

where $N_{v,GEM}^{trop}$ is the monthly averaged GEM-AQ model-based tropospheric $NO_2$ column number density, $N_{v,TROPOMI}^{trop}$ is the monthly averaged TROPOMI-based tropospheric $NO_2$ column number density, $a$ and $b$ are regression parameters.
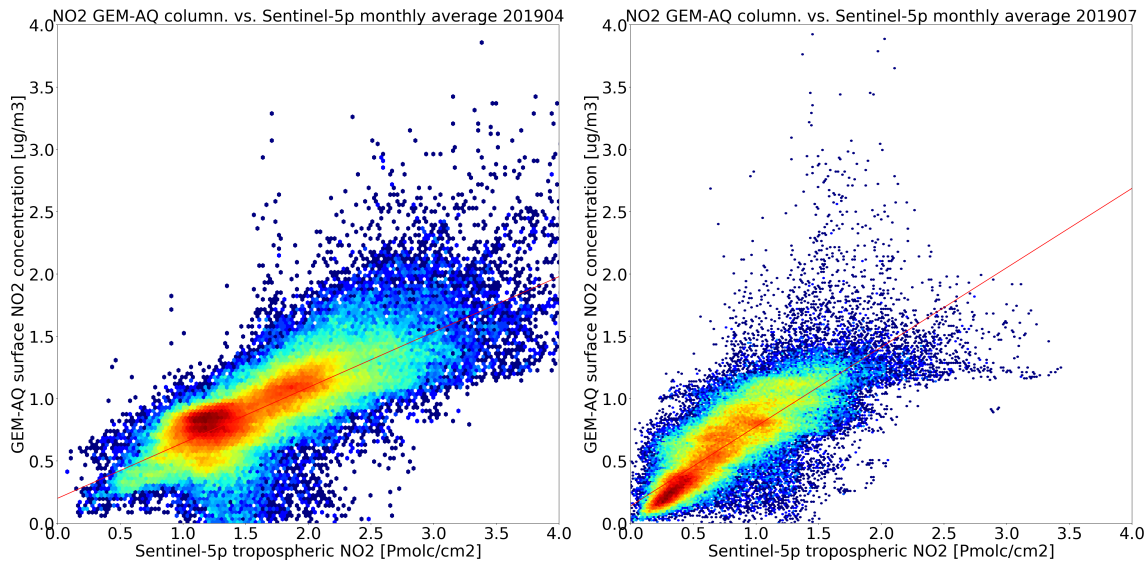
**Figure 3.** Scatter plots of monthly averaged tropospheric column retrieved by TROPOMI (horizontal axis) and GEM-AQ model (vertical axis) for **(A)**April and **(B)**July

**Table 1.** Parameters of equation 4, fitted to monthly averaged tropospheric column rasters; goodness of fit for each monthly average

| Month | a | b | $R^2$ | $MSE$ |
|---|---|---|---|---|
| January | 1.4 | 0.28 | 0.13 | 1.29 |
| February | 0.92 | 0.3 | 0.36 | 0.67 |
| March | 0.38 | 0.44 | 0.36 | 0.11 |
| April | 0.45 | 0.2 | 0.53 | 0.05 |
| May | 0.42 | 0.23 | 0.59 | 0.06 |
| June | 0.51 | 0.22 | 0.37 | 0.04 |
| July | 0.64 | 0.14 | 0.66 | 0.04 |
| August | 0.59 | 0.15 | 0.45 | 0.04 |
| September | 0.54 | 0.29 | 0.52 | 0.06 |
| October | 0.75 | 0.06 | 0.63 | 0.14 |
| November | 0.78 | 0.09 | 0.5 | 0.48 |
| December | 0.8 | 0.58 | 0.4 | 0.69 |

Table 1 summarises fitting results. The best (in terms of high $R^2$ and low MSE) linear regression was obtained for the July monthly average tropospheric column. The MSE value follows the pattern - low during summer months, higher during winter months. $R^2$ does not seem to reveal any annual pattern. Thus it is either cloud cover or emission underestimation, making GEM-AQ and TROPOMI tropospheric column slightly different.

Both scatter plots (fig. 3) and regression parameters ($a < 1$) suggest that except for winter months, on a regional scale GEM-AQ model underestimates the $NO_2$ tropospheric column number densities. However, it is still questionable at this stage if it is overestimated caused by TROPOMI or underestimation by GEM-AQ.

### 3.2. The choice of qa_value

TROPOMI $NO_2$ OFFL product was processed by the DOMINO algorithm (version 1.2) on the ESA side. One of the auxiliary outputs of this algorithm is the quality assurance flag (qa_value). According to TROPOMI NO2 ATBD [38], the threshold of 0.75 should be used to remove clouds, pixels covered by snow and other problematic retrievals. Setting the threshold at 0.75 is sufficient for summer months, however in winter (November - February), only a few (less than 10) satellite images per month satisfy

this condition (fig. 4 C,D). Reducing $qa_value$ threshold to 0.7 or 0.5 may lead to some improvement (fig. 4 A,B). However, a lower threshold leads to underestimation in comparison to modelling results (fig. 8).
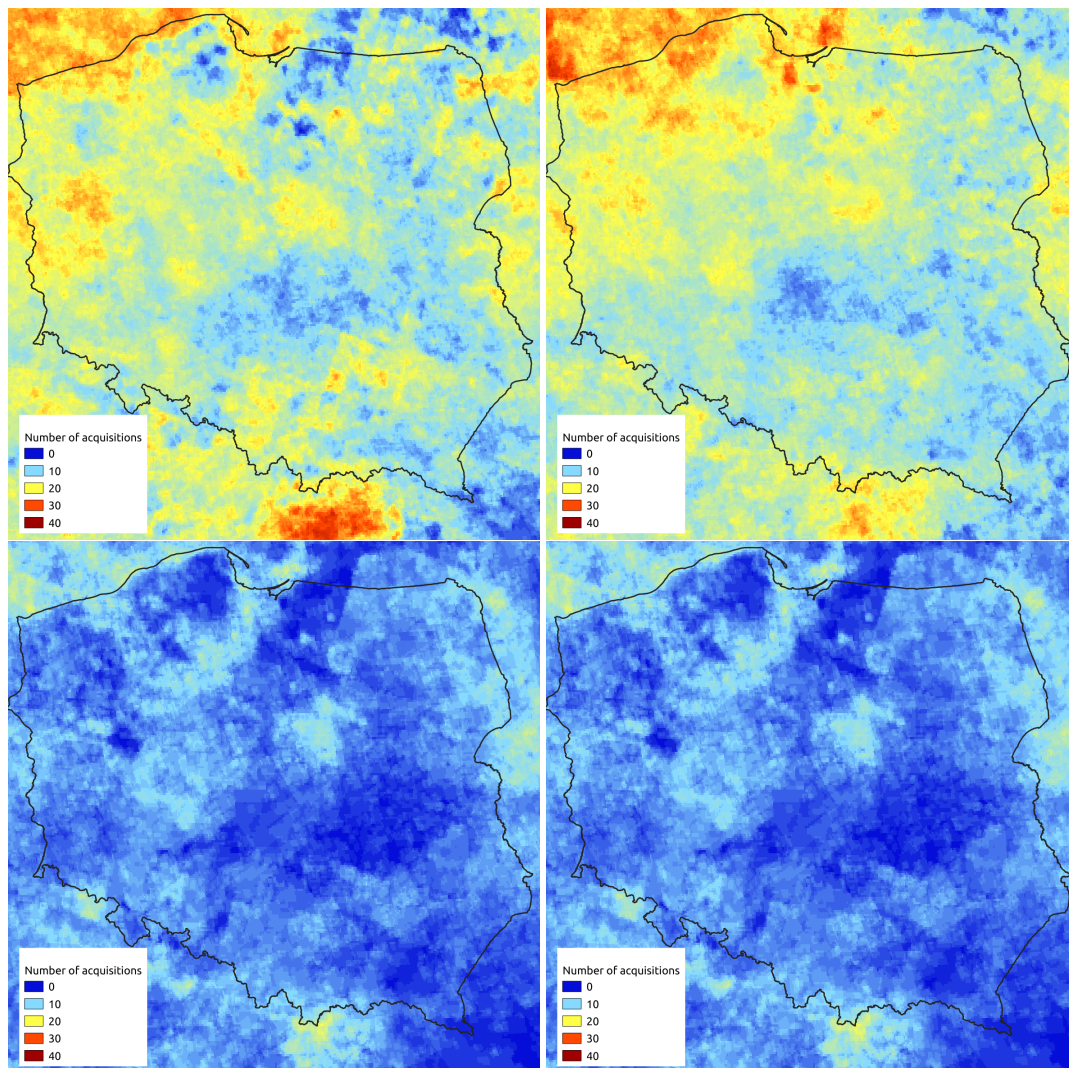


**Figure 4.** Number of pixels available for monthly averaging in January 2019 for given $qa\_value$ threshold **(a)**0.5 **(b)**0.7 **(c)**0.75 **(d)**0.8

*3.3. Spatial Distribution*

We investigated the spatial distribution of $NO_2$. As figure 5 shows, the monthly averaged TROPOMI tropospheric $NO_2$ column reproduces the locations of significant $NO_x$ point sources. At the same time, this spatial pattern is not reproduced in the GEM-AQ surface layer. This confirms the fact that the TROPOMI instrument at the satellite level is not sensitive to surface layers. The only location where TROPOMI tropospheric column seems to be better correlated with surface concentration than with GEM-AQ tropospheric column is the coastal area, near the city of Gdańsk. Although no significant $NO_x$ point sources are located there - relatively high values of $NO_2$ column number density on the TROPOMI column (fig. 5 A) and model-based $NO_2$ surface concentration (fig. 6 B) can be noticed near the city of Gdańsk. This fact may be explained by harbour emission, which may be underestimated in the GEM-AQ model. Due to local sea-breeze circulation, the whole tropospheric column could be well mixed.
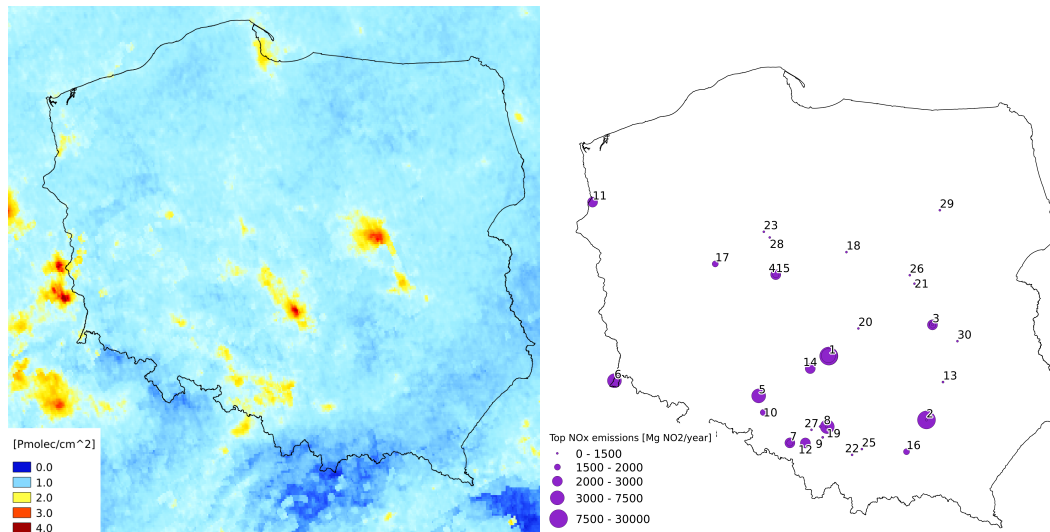
**Figure 5.** (**A**)Satellite distribution of $NO_2$ tropospheric column density (monthly average - June 2019) (B) Locations of top 30 $NO_x$ emission point sources in Poland.
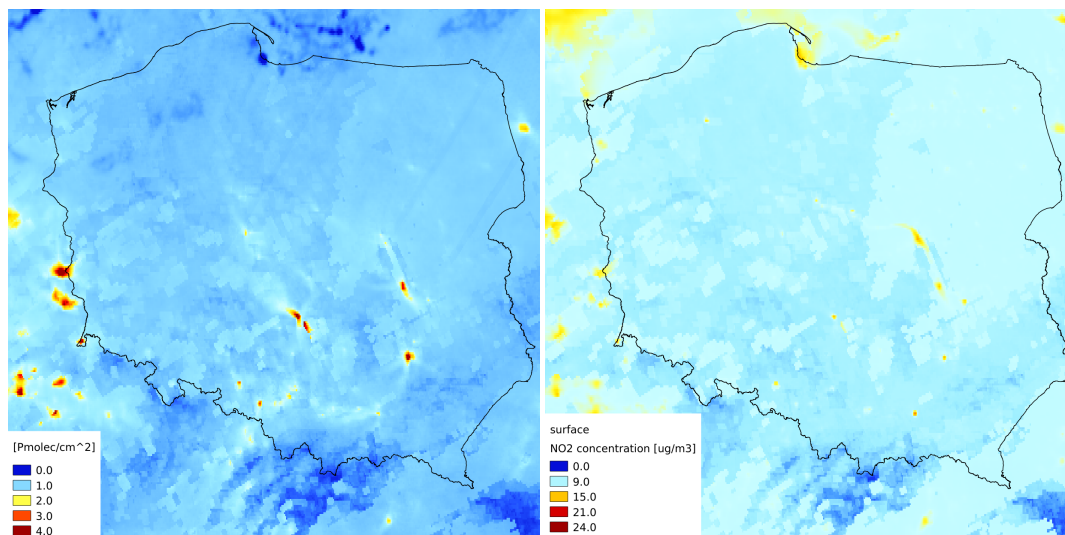


**Figure 6.** (**A**) GEM-AQ model-based $NO_2$ tropospheric column density (monthly average - June 2019) (B) GEM-AQ model-based $NO_2$ concentration at surface level (monthly average - June 2019)

The troposphere $NO_2$ column number density reveals the locations of primary point sources and the dominant wind direction. As the monthly average tropospheric $NO_2$ column is an average of non-cloudy days (mornings), the resulting spatial distribution depends on accidental wind direction. Comparison of model-based and satellite-borne tropospheric $NO_2$ column over the whole domain (like fig. 3 and eq. 4) may be biased by a small error in modelled wind direction, leading to wrong concentration distribution.

To make the comparison less wind-depended, we extracted the troposphere column number density value from pixels surrounding locations of the fifteen major point emitters (fig.5B) from both TROPOMI results and the GEM-AQ model. Yearly-averaged values for GEM-AQ and TROPOMI in most cases agree within the margin of 15%. Only in the case of three emitters (out of fifteen) the GEM-AQ model seems to underestimate tropospheric column number density; in other cases, a slight overestimation by the model is visible (fig. 7).
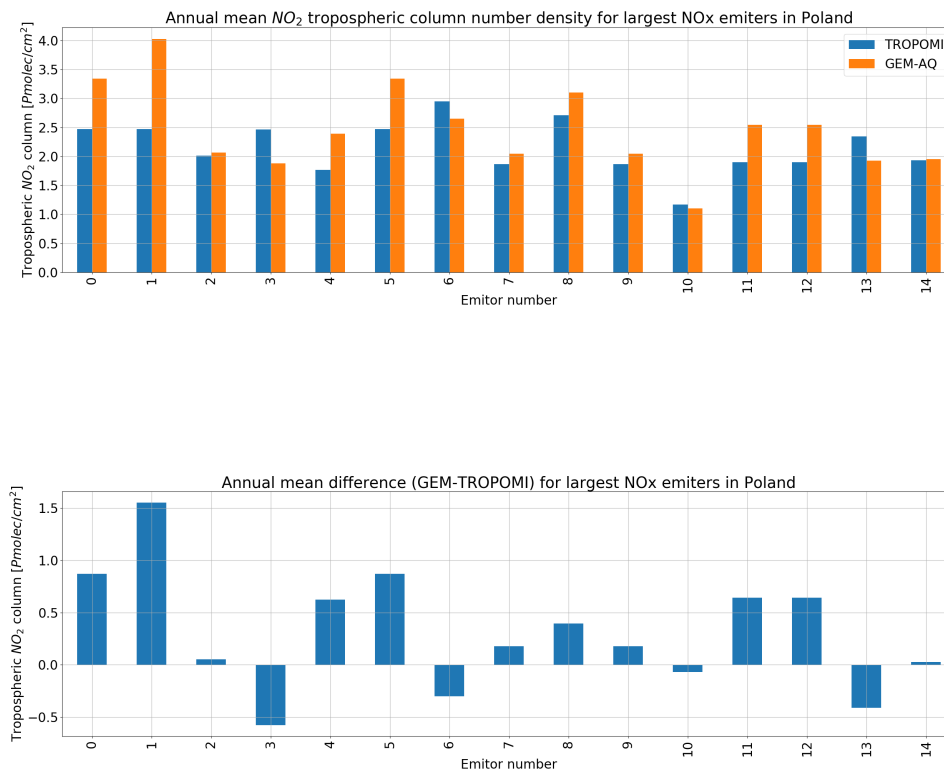
**Figure 7.** **(A)** Annual mean tropospheric $NO_2$ column number density extracted from pixels surrounding fifteen largest point emitters, from both TROPOMI acquisition and the GEM-AQ model. **(B)** Annual mean difference between GEM-AQ and TROPOMI tropospheric column for fifteen largest emitters; Emitter numbers are the same as in figure 5

*3.4. Temporal Comparison*

Both $NO_x$ emissions and $NO_2$ concentrations follow the same annual pattern - low in summer and high in winter. This fact is due to higher energy demand and low wind velocity episodes during the winter months. Moreover, some of the largest coal-burning power plants in Poland are also sources of heat for city-wide heating systems. Thus they do burn more coal during low temperatures periods.

Because of cloud cover and non-point sources (road traffic), we decided to analyse the temporal pattern only over the largest $NO_x$ emitters. The difference between GEM-AQ tropospheric column and TROPOMI tropospheric column seems to be the smallest during the summer months (less than $0.5 Pmolec/cm^2$, fig 8). In autumn, the difference starts to grow, and it exceeds $1.0 Pmolec/cm^2$ in December.

The choice of the *qa_value* threshold seems to have a significant influence in January and February. For *qa_value*=0.5, TROPOMI returns higher values than the GEM-AQ model. This is probably due to partial cloud cover, which would have been filtered out when a higher *qa_value* is chosen. Regardless of the *qa_value* April and May $NO_2$ column concentrations seem to be underestimated in the GEM-AQ model, which may be caused by an overestimated ozone production during these months.
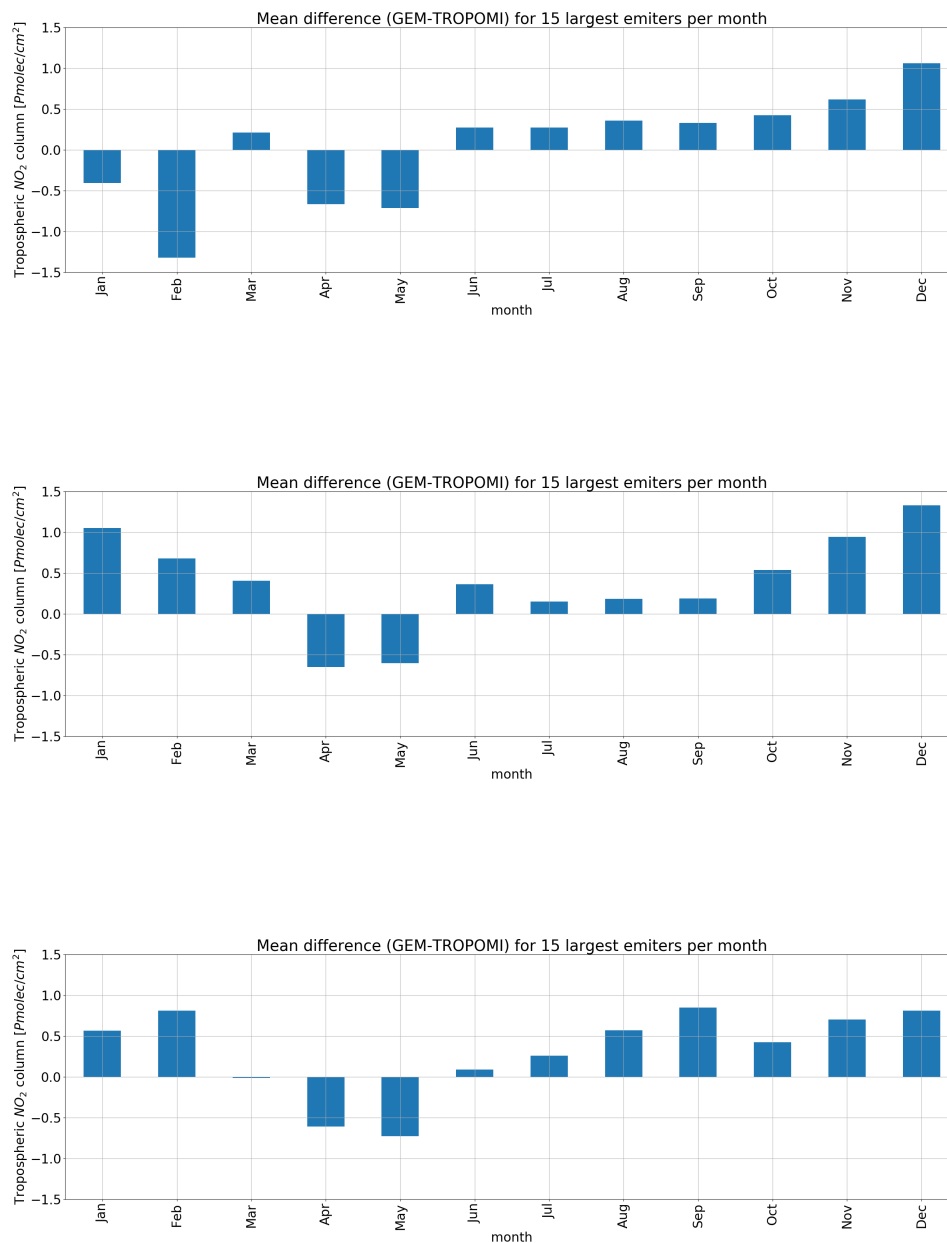
**Figure 8.** Mean difference in tropospheric column number density per month for different *qa_value* threshold: **(A)***qa_value* = 0.5,**(B)***qa_value* = 0.7,**(C)***qa_value* = 0.75

### 3.5. Relation to near-surface concentration

Although there are authors [2] who present linear relation between the near-surface concentration and $NO_2$ tropospheric column, according to averaging kernel vertical distribution, the TROPOMI instrument is not very sensitive to $NO_2$ concentration at surface level (fig.2). It is probably hindered by the sensitivity at higher levels of the troposphere. Therefore a more complex relation linking $NO_2$ near-surface concentration and the tropospheric column is needed.

A concept of explaining tropospheric $NO_2$ column density using nonlinear regression against surface concentration and boundary layer depth was introduced by Dieudonne et al.[46]. Further on, it was applied to TROPOMI data over Paris by Lorrente [22], who showed that $NO_2$ surface
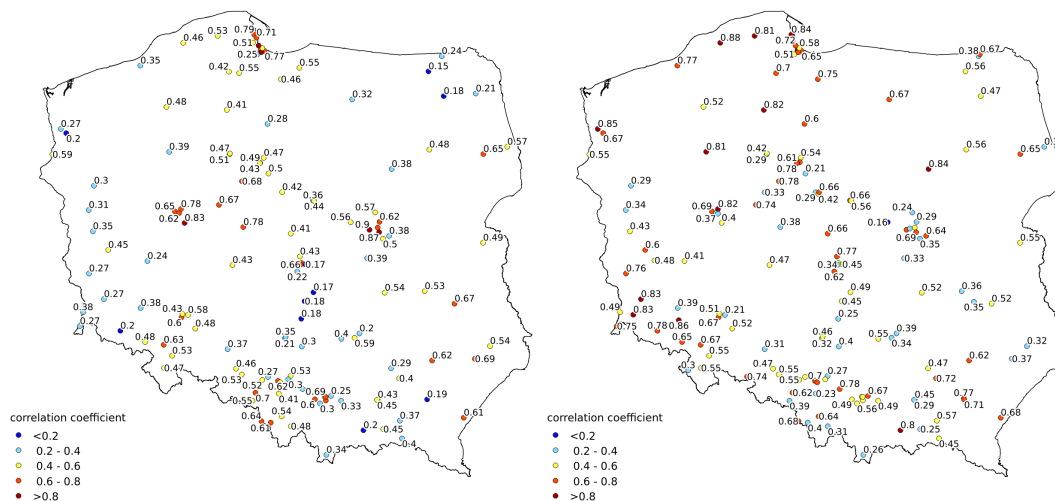
**Figure 9.** The correlation coefficient for nonlinear regression equation 6 in **(A)**April 2019 and **(B)** September 2019

concentration $c_{surf}$, tropospheric vertical column number density $N_v^{trop}$ and boundary layer depth $h$ the following empirical equation:

$$N_v^{trop} = K[0.244h(c_{surf} - 1.38) + 0.184(c_{surf} - 2.83)] \tag{5}$$

where $K$ is a constant conversion factor ($1.31 \cdot 10^{15} molc/cm^2$). We decided to introduce a more general nonlinear equation:

$$N_v^{trop} = [(a \cdot h + b) \cdot c_{surf} - c \cdot h + d] \tag{6}$$

Parameters of equation 6 were fitted using Levenberg–Marquardt algorithm[47]. Fitting was performed separately for each measurement station in each month. Stations where the number of TROPOMI tropospheric column values were lower than ten were discarded. Therefore the results were highly dependent on cloud conditions. The best results were obtained for April and September 2019 (fig. 9). The spatial pattern of the correlation coefficient reveals that equation 6 performs reasonably well within larger cities and densely populated areas (fig. 9). This is probably caused by the more significant contribution of road traffic $NO_x$ emissions to the tropospheric $NO_2$ VCD.

## 4. Conclusions

Over the operational air quality forecast domain, performed routinely using the GEM-AQ model, we examined the results of the latest fine-scale satellite instrument (TROPOMI aboard Sentinel-5P) from the year 2019. The key findings from this study are the following:

1. In general, the GEM-AQ model tends to underestimate the $NO_2$ tropospheric column number density, which may be caused by either too intense mixing in the atmosphere, a sink of $NO_2$ into further chemical processes (e.g. tropospheric ozone production) or too small background concentration

2. When looking at locations next to the largest $NO_x$ point emitters in Poland, the GEM-AQ model and TROPOMI converge reasonably well. Minor differences should be explained by individual emission examination

3. The TROPOMI instrument does not correctly reproduce the annual temporal concentration pattern. It seems that cloud cover (thus *qa_value* threshold) and the number of satellite scenes averaged into monthly average play an important role. Lowering the *qa_value* during the

summer months improve the convergence between TROPOMI and GEM-AQ, while during the winter months, it acts oppositely.

4. The relation between near surface concentration and troposphere column number density can be parametrised using boundary layer depth as an additional explanatory variable.

We conclude TROPOMI is powerful and independent from the ground measurements source of $NO_2$ distribution data from the above findings. Although column number density is not to be used directly with surface concentration, it is still helpful for validating modelling results. After some additional processing, TROPOMI $NO_2$ column number densities can also be used for estimating near-surface concentrations in urban areas.

In further works, we would like to broaden our studies to model runs with different emission inventories - CAMS and EMEP. An interesting follow-up would also be developing a data assimilation scheme for the GEM-AQ model capable of assimilating TROPOMI $NO_2$ VCDs into the GEM-AQ model.

1. Atkinson, R. Atmospheric chemistry of VOCs and NOx. *Atmospheric environment* **2000**, *34*, 2063–2101.
2. Zheng, Z.; Yang, Z.; Wu, Z.; Marinello, F. Spatial Variation of NO2 and Its Impact Factors in China: An Application of Sentinel-5P Products. *Remote Sensing* **2019**, *11*, 1939.
3. Beloconi, A.; Vounatsou, P. Bayesian geostatistical modelling of high-resolution NO2 exposure in Europe combining data from monitors, satellites and chemical transport models. *Environment International* **2020**, *138*, 105578.
4. Curier, R.; Kranenburg, R.; Segers, A.; Timmermans, R.; Schaap, M. Synergistic use of OMI NO2 tropospheric columns and LOTOS–EUROS to evaluate the NOx emission trends across Europe. *Remote sensing of environment* **2014**, *149*, 58–69.
5. Hoogen, R.; Rozanov, V.V.; Burrows, J.P. Ozone profiles from GOME satellite data: Algorithm description and first validation. *Journal of Geophysical Research: Atmospheres* **1999**, *104*, 8263–8280.
6. Rozanov, A.; Bovensmann, H.; Bracher, A.; Hrechanyy, S.; Rozanov, V.; Sinnhuber, M.; Stroh, F.; Burrows, J. NO2 and BrO vertical profile retrieval from SCIAMACHY limb measurements: Sensitivity studies. *Advances in space research* **2005**, *36*, 846–854.
7. Valks, P.; Pinardi, G.; Richter, A.; Lambert, J.C.; Hao, N.; Loyola, D.; Van Roozendael, M.; Emmadi, S. Operational total and tropospheric NO2 column retrieval for GOME-2. *Atmospheric Measurement Techniques* **2011**, *4*, 1491.
8. Russell, A.R.; Valin, L.C.; Bucsela, E.J.; Wenig, M.O.; Cohen, R.C. Space-based Constraints on Spatial and Temporal Patterns of NO x Emissions in California, 2005- 2008. *Environmental science & technology* **2010**, *44*, 3608–3615.
9. Duncan, B.N.; Yoshida, Y.; de Foy, B.; Lamsal, L.N.; Streets, D.G.; Lu, Z.; Pickering, K.E.; Krotkov, N.A. The observed response of Ozone Monitoring Instrument (OMI) NO2 columns to NOx emission controls on power plants in the United States: 2005–2011. *Atmospheric Environment* **2013**, *81*, 102–111.
10. Castellanos, P.; Boersma, K.F. Reductions in nitrogen oxides over Europe driven by environmental policy and economic recession. *Scientific reports* **2012**, *2*, 265.
11. Duncan, B.N.; Lamsal, L.N.; Thompson, A.M.; Yoshida, Y.; Lu, Z.; Streets, D.G.; Hurwitz, M.M.; Pickering, K.E. A space-based, high-resolution view of notable changes in urban NOx pollution around the world (2005–2014). *Journal of Geophysical Research: Atmospheres* **2016**, *121*, 976–996.
12. De Foy, B.; Lu, Z.; Streets, D.G. Satellite NO 2 retrievals suggest China has exceeded its NO x reduction goals from the twelfth Five-Year Plan. *Scientific reports* **2016**, *6*, 1–9.
13. Lin, J.; Nielsen, C.P.; Zhao, Y.; Lei, Y.; Liu, Y.; McElroy, M.B. Recent changes in particulate air pollution over China observed from space and the ground: effectiveness of emission control. *Environmental science & technology* **2010**, *44*, 7771–7776.
14. de Ruyter de Wildt, M.; Eskes, H.; Boersma, K.F. The global economic cycle and satellite-derived NO2 trends over shipping lanes. *Geophysical research letters* **2012**, *39*.

15.    Zhang, X.; Zhang, W.; Lu, X.; Liu, X.; Chen, D.; Liu, L.; Huang, X.  Long-term trends in NO2 columns related to economic developments and air quality policies from 1997 to 2016 in China. *Science of the Total Environment* **2018**, *639*, 146–155.

16.    Du, Y.; Xie, Z. Global financial crisis making a V-shaped fluctuation in NO 2 pollution over the Yangtze River Delta. *Journal of Meteorological Research* **2017**, *31*, 438–447.

17.    Mijling, B.; Van Der A, R.; Boersma, K.; Van Roozendael, M.; De Smedt, I.; Kelder, H.  Reductions of NO2 detected from space during the 2008 Beijing Olympic Games. *Geophysical Research Letters* **2009**, *36*.

18.    Saw, G.K.; Dey, S.; Kaushal, H.; Lal, K.  Tracking NO2 emission from thermal power plants in North India using TROPOMI data. *Atmospheric Environment* **2021**, p. 118514.

19.    Skoulidou, I.; Koukouli, M.E.; Segers, A.; Manders, A.; Balis, D.; Stavrakou, T.; van Geffen, J.; Eskes, H. Changes in Power Plant NOx Emissions over Northwest Greece Using a Data Assimilation Technique **2021**.

20.    Hakkarainen, J.; Szeląg, M.E.; Ialongo, I.; Retscher, C.; Oda, T.; Crisp, D.  Analyzing nitrogen oxides to carbon dioxide emission ratios from space: A case study of Matimba Power Station in South Africa. *Atmospheric Environment: X* **2021**, *10*, 100110.

21.    Borsdorff, T.; García Reynoso, A.; Maldonado, G.; Mar-Morales, B.; Stremme, W.; Grutter, M.; Landgraf, J. Monitoring CO emissions of the metropolis Mexico City using TROPOMI CO observations. *Atmospheric Chemistry and Physics* **2020**, *20*, 15761–15774.

22.    Lorente, A.; Boersma, K.; Eskes, H.; Veefkind, J.; Van Geffen, J.; de Zeeuw, M.; van der Gon, H.D.; Beirle, S.; Krol, M. Quantification of nitrogen oxides emissions from build-up of pollution over Paris with TROPOMI. *Scientific reports* **2019**, *9*, 1–10.

23.    Goldberg, D.L.; Lu, Z.; Streets, D.G.; de Foy, B.; Griffin, D.; McLinden, C.A.; Lamsal, L.N.; Krotkov, N.A.; Eskes, H.  Enhanced Capabilities of TROPOMI NO2: Estimating NO X from North American Cities and Power Plants. *Environmental science & technology* **2019**, *53*, 12594–12601.

24.    de Laat, A.; Ding, J.; Eskes, H.; others.  Connecting the dots: NO x emissions along a West Siberian natural gas pipeline. *npj Climate and Atmospheric Science* **2020**, *3*, 1–7.

25.    Lu[1], G.; Marais, E.A.; Vohra[1], K.; Zhu, L.  Shipping Emissions in Rapidly Growing Seaports in Africa Determined with TROPOMI.

26.    McLinden, C.; Fioletov, V.; Griffin, D.; Dammers, E.  High-resolution mapping of NOx emissions from the Canadian Oil Sands from TROPOMI. EGU General Assembly Conference Abstracts, 2020, p. 3959.

27.    Tack, F.; Merlaud, A.; Iordache, M.D.; Pinardi, G.; Dimitropoulou, E.; Eskes, H.; Bomans, B.; Veefkind, P.; Van Roozendael, M.  Assessment of the TROPOMI tropospheric NO 2 product based on airborne APEX observations. *Atmospheric Measurement Techniques* **2021**, *14*, 615–646.

28.    Judd, L.M.; Al-Saadi, J.A.; Szykman, J.J.; Valin, L.C.; Janz, S.J.; Kowalewski, M.G.; Eskes, H.J.; Veefkind, J.P.; Cede, A.; Mueller, M.; others.  Evaluating Sentinel-5P TROPOMI tropospheric NO 2 column densities with airborne and Pandora spectrometers near New York City and Long Island Sound. *Atmospheric Measurement Techniques* **2020**, *13*, 6113–6140.

29.    Dimitropoulou, E.; Hendrick, F.; Pinardi, G.; Friedrich, M.M.; Merlaud, A.; Tack, F.; De Longueville, H.; Fayt, C.; Hermans, C.; Laffineur, Q.; others.  Validation of TROPOMI tropospheric NO 2 columns using dual-scan multi-axis differential optical absorption spectroscopy (MAX-DOAS) measurements in Uccle, Brussels. *Atmospheric Measurement Techniques* **2020**, *13*, 5165–5191.

30.    Verhoelst, T.; Compernolle, S.; Pinardi, G.; Lambert, J.C.; Eskes, H.J.; Eichmann, K.U.; Fjæraa, A.M.; Granville, J.; Niemeijer, S.; Cede, A.; others.   Ground-based validation of the Copernicus Sentinel-5P TROPOMI NO2 measurements with the NDACC ZSL-DOAS, MAX-DOAS and Pandonia global networks **2021**.

31.    Ialongo, I.; Virta, H.; Eskes, H.; Hovila, J.; Douros, J.  Comparison of TROPOMI/Sentinel-5 Precursor NO 2 observations with ground-based measurements in Helsinki. *Atmospheric Measurement Techniques* **2020**, *13*, 205–218.

32.    Boersma, K.; Eskes, H.; Dirksen, R.; Veefkind, J.; Stammes, P.; Huijnen, V.; Kleipool, Q.; Sneep, M.; Claas, J.; Leitão, J.; others.  An improved tropospheric NO 2 column retrieval algorithm for the Ozone Monitoring Instrument. *Atmospheric Measurement Techniques* **2011**, *4*, 1905–1928.

33. Lorente, A.; Boersma, K.F.; Yu, H.; Dörner, S.; Hilboll, A.; Richter, A.; Liu, M.; Lamsal, L.N.; Barkley, M.; De Smedt, I.; others. Structural uncertainty in air mass factor calculation for NO2 and HCHO satellite retrievals. *Atmospheric Measurement Techniques* **2017**, *10*, 759–782.

34. Williams, J.E.; Boersma, K.F.; Le Sager, P.; Verstraeten, W.W. The high-resolution version of TM5-MP for optimized satellite retrievals: description and validation. *Geoscientific Model Development* **2017**, *10*, 721–750.

35. Van Geffen, J.; Boersma, K.F.; Eskes, H.; Sneep, M.; Ter Linden, M.; Zara, M.; Veefkind, J.P. S5P TROPOMI NO2 slant column retrieval: method, stability, uncertainties and comparisons with OMI. *Atmospheric Measurement Techniques* **2020**, *13*.

36. Kim, H.C.; Kim, S.; Lee, S.H.; Kim, B.U.; Lee, P. Fine-Scale Columnar and Surface NOx Concentrations over South Korea: Comparison of Surface Monitors, TROPOMI, CMAQ and CAPSS Inventory. *Atmosphere* **2020**, *11*, 101.

37. Griffin, D.; Griffin, D.; Zhao, X.; McLinden, C. High resolution mapping of nitrogen dioxide with TROPOMI: First results and validation over the Canadian oil sands. *Geophysical Research Letters* **2018**, *45*.

38. van Geffen, J.; Eskes, H.; Boersma, K.; Maasakkers, J.; Veefkind, J. TROPOMI ATBD of the total and tropospheric NO2 data products (issue 1.2. 0). *Royal Netherlands Meteorological Institute (KNMI), De Bilt, the Netherlands, s5P-KNMI-L2-0005-RP* **2018**.

39. Niemeijer, S. ESA Atmospheric Toolbox. EGU General Assembly Conference Abstracts, 2017, Vol. 19, p. 8286.

40. Côté, J.; Gravel, S.; Méthot, A.; Patoine, A.; Roch, M.; Staniforth, A. The operational CMC–MRB global environmental multiscale (GEM) model. Part I: Design considerations and formulation. *Monthly Weather Review* **1998**, *126*, 1373–1395.

41. Venkatram, A.; Karamchandani, P.; Misra, P. Testing a comprehensive acid deposition model. *Atmospheric Environment (1967)* **1988**, *22*, 737–747.

42. Kaminski, J.; Neary, L.; Struzewska, J.; McConnell, J.; Lupu, A.; Jarosz, J.; Toyota, K.; Gong, S.; Côté, J.; Liu, X.; others. GEM-AQ, an on-line global multiscale chemical weather modelling system: model description and evaluation of gas phase chemistry processes. *Atmospheric chemistry and physics* **2008**, *8*, 3255–3281.

43. Szymankiewicz, K.; Kaminski, J.W.; Struzewska, J. Interannual variability of tropospheric NO 2 column over Central Europe—Observations from SCIAMACHY and GEM-AQ model simulations. *Acta Geophysica* **2014**, *62*, 915–929.

44. Tagaris, E.; Sotiropoulou, R.E.P.; Gounaris, N.; Andronopoulos, S.; Vlachogiannis, D. Effect of the Standard Nomenclature for Air Pollution (SNAP) categories on air quality over Europe. *Atmosphere* **2015**, *6*, 1119–1128.

45. Stull, R.B. *An introduction to boundary layer meteorology*; Vol. 13, Springer Science & Business Media, 2012.

46. Dieudonné, E.; Ravetta, F.; Pelon, J.; Goutail, F.; Pommereau, J.P. Linking NO2 surface concentration and integrated content in the urban developed atmospheric boundary layer. *Geophysical research letters* **2013**, *40*, 1247–1251.

47. Levenberg, K. A method for the solution of certain non-linear problems in least squares. *Quarterly of applied mathematics* **1944**, *2*, 164–168.